

**Optical phase noise from atmospheric fluctuations and its impact on optical time-frequency transfer**L. C. Sinclair,\* F. R. Giorgetta, W. C. Swann, E. Baumann, I. Coddington, and N. R. Newbury  
*National Institute of Standards and Technology, 325 Broadway, Boulder, Colorado 80305, USA*

(Received 9 December 2013; published 5 February 2014)

The time of flight for a laser beam through the atmosphere will fluctuate as the path-averaged index of refraction varies with atmospheric turbulence, air temperature, and pressure. We measure these fluctuations by transmitting optical pulses from a frequency comb across a 2-km horizontal path and detecting variations in their time of flight through linear optical sampling. This technique is capable of continuous measurements, with femtosecond resolution, over time scales of many hours despite turbulence-induced signal fading. The power spectral density for the time of flight, or equivalently for the optical phase, follows a simple power-law response of  $\propto f^{-2.3}$  measured down to Fourier frequencies,  $f$ , of 100  $\mu\text{Hz}$ . There is no evidence of a roll-off at low frequencies associated with an outer scale for turbulence. Both of these results depart from the predictions of turbulence theory, but are consistent with some other results in the literature. We discuss the implications for the stability and accuracy of one-way optical time-frequency transfer.

DOI: [10.1103/PhysRevA.89.023805](https://doi.org/10.1103/PhysRevA.89.023805)

PACS number(s): 42.25.Dd, 42.68.Bz

**I. INTRODUCTION**

The impact of atmospheric turbulence on the propagation of light through the atmosphere is well studied [1–5]. It will cause both strong intensity fluctuations and strong phase fluctuations at a receiver. The intensity fluctuations are perhaps the most obvious consequence and lead to intermittent, strong signal fading in coherent free-space communication links. However, for a number of applications, optical phase fluctuations are equally fundamental and equally detrimental. The optical phase noise leads to variations in the time of flight of a laser beam, with consequences for laser ranging, optical time-frequency transfer, and long-baseline interferometry. It also leads to angle-of-arrival variations and higher-order distortions of the optical wave front, which can limit the quality of seeing for astronomy and free-space laser communications links.

In this paper, we present experimental measurements of the optical phase noise power spectral density (PSD), as measured by time of flight of optical pulses from a laser frequency comb across a 2-km horizontal path. These data were acquired in the course of an experiment on two-way optical time-frequency transfer [6] and reanalyzed here to evaluate the magnitude of the atmospheric phase noise. This time-of-flight measurement is sensitive to the same atmospheric phase noise effects as the optical carrier phase but, unlike cw laser interferometry, can probe the phase noise across time scales extending to many hours, i.e., Fourier frequencies as low as 100  $\mu\text{Hz}$ . We find that the optical phase noise PSD exhibits a single power-law decay at  $f^{-2.3}$ , where  $f$  is the Fourier frequency, over five orders of magnitude in frequency with no roll-off in the PSD at low frequencies.

This simple power law is surprising in the context of standard turbulence theory, which predicts both a steeper power-law scaling at intermediate frequencies and a “flattening” of the PSD at low frequencies due to the presence of an outer length scale for turbulence. However, this prediction is based on some central assumptions of questionable validity, especially

at low Fourier frequencies. Specifically, the derivation makes use of Taylor’s hypothesis, which assumes that the turbulence spatial structure is frozen, so that the only time dependence arises from the wind [7]. Other results in the literature have also found shallower power-law scaling and an absence of a low-frequency roll-off [8–15], although none have probed the atmospheric optical phase noise on as long a time scale. Nevertheless, the power-law scaling observed here over a full five orders of magnitude is a strikingly simple result particularly when considered in the light of the full complexity of turbulence and weather.

The optical phase PSD is important for evaluation of a number of systems including laser ranging [16,17] and long-baseline interferometry [12,18–20]. Our motivation here, as in Refs. [6,14,21], is free-space optical time-frequency transfer. Optically based transfer over fiber is quite successful [22–34], but does require installed optical fiber between the end locations. Optical time-frequency transfer over free-space removes this constraint, but will suffer the effects of atmospheric phase noise. Based on the data here, the limitations imposed by turbulence and weather on the stability of one-way optical time-frequency transfer are indeed severe. As shown, even over the relatively short 2-km path, the modified Allan deviation is limited from  $10^{-14}$  to  $10^{-15}$  from a few seconds to 1000 s. Perhaps more importantly, weather will lead to linear temperature gradients that cause long-term changes in optical path length that increase linearly with air-path distance and are already at the  $10^{-14}$ – $10^{-15}$  level over only 2 km, for 0.5–5  $^{\circ}\text{C}/\text{h}$ . Fortunately, as part of the same experiment discussed here, we demonstrated that this atmospheric phase noise can be canceled to a residual fractional accuracy below  $10^{-18}$  through a two-way technique that relies on reciprocity of single-mode links [6]. For other applications, such as laser-based ranging or long-baseline interferometry, the optical phase noise PSD measured here cannot be similarly suppressed, and the absence of a roll-off in the PSD down to 100- $\mu\text{Hz}$  Fourier frequencies indicates that increasing measurement periods from minutes to hours will not mitigate its effect. Certainly, the PSD must roll off at some lower Fourier frequency, but it may be impractical to extend the measurement period to that long of a time scale.

\*laura.sinclair@nist.gov

In the remainder of this paper, Sec. II reviews the theoretical background for the expected optical phase noise PSD and related quantities. Section III discusses the experimental setup. Section IV presents the measured PSDs for the time of flight as well as the angle-of-arrival fluctuations and carrier-phase noise. Section V discusses the results, compares them with theory and other related efforts in the literature, and finally analyzes their impact on optical time-frequency transfer. Section VI concludes with a summary of the main results and their implications.

## II. THEORETICAL BACKGROUND

In this section, we briefly review the well-established theoretical work on atmospheric optical phase noise [2–5,35–39]. The variation in the time of flight of an optical signal across a path of length  $L$  is  $\delta x(t) = c^{-1} \int_0^L \delta n(z,t) dz$ , where  $c$  is the vacuum speed of light and the optical beam travels in the  $z$  direction. For optical pulses,  $\delta n(z,t)$  is the variation in the group index of refraction, while for an optical carrier,  $\delta n(z,t)$  is the variation in the phase index of refraction, but the two differ by only  $\sim 10^{-3}$  at  $1.5 \mu\text{m}$  [40]. The corresponding optical phase noise is  $\delta\phi(t) = 2\pi\nu_0\delta x(t)$  for an optical carrier frequency,  $\nu_0$ . Turbulence theory develops an expression for  $\delta n(z,t)$  and, from that, derives the PSD of the phase noise and related quantities.

Initial theoretical descriptions focused on  $\delta n(z,t)$  from turbulent eddies in the inertial region, defined between an outer length scale,  $L_0$ , where energy is injected into the system, down to an inner length scale,  $l_0$ , where dissipative loss dominates. Different estimates of the outer scale  $L_0$  appear in the literature of  $L_0 \sim 0.4h$ ,  $L_0 \sim 2\sqrt{h}$ , or  $L_0 \sim h$ , where  $h$  is the height of the optical path above the ground [3,9,35,41]. The inner length scale,  $l_0$ , is a few mm. Over this inertial region, Tatarski gave the Kolmogorov spectrum of spatial fluctuations in the index of refraction as

$$\Phi_n(\kappa) = 0.033C_n^2\kappa^{-11/3} \quad 2\pi/L_0 < \kappa < 2\pi/l_0, \quad (1)$$

where  $C_n^2$  is the turbulence structure constant and  $\kappa$  is the magnitude of the spatial frequency [35]. Attempts have been made to extend the Kolmogorov spectrum to scales beyond both the outer scale (i.e., to lower spatial frequencies) and the inner scale (i.e., to higher spatial frequencies). The mathematically convenient von Karman spectrum is

$$\Phi_n(\kappa) = 0.033C_n^2[\kappa^2 + (1/L_0)^2]^{-11/6} \exp(-\kappa^2/\kappa_m^2) \quad 0 < \kappa < \infty, \quad (2)$$

where  $\kappa_m = 5.92/l_0$  [2]. Through actual measurements of the microtemperature variations, Greenwood and Tarazano developed the empirical spectrum [38],

$$\Phi_n(\kappa) = 0.033C_n^2[\kappa^2 + (\kappa/L_0)^2]^{-11/6} \quad 0 < \kappa < 2\pi/l_0, \quad (3)$$

further supported in later measurements by Wheelon *et al.* [18]. Both of these extensions maintain the  $\kappa^{-11/3}$  scaling over the inertial subrange.

Under Taylor's hypothesis of frozen turbulence with a constant wind speed,  $V$ , perpendicular to the beam direction, the three-dimensional spatial spectrum,  $\Phi_n(\kappa)$ , is converted for plane wave propagation to a one-dimensional temporal PSD,

$S_\phi(f)$  [7,39]. The Kolmogorov spectrum yields

$$S_\phi(f) = 0.016k^2C_n^2LV^{5/3}f^{-8/3} \quad [\text{rad}^2/\text{Hz}], \quad (4)$$

where  $f$  is a temporal frequency,  $L$  is the total path length, and  $k$  is the wave number. The von Karman spectrum yields

$$S_\phi(f) = 0.016k^2LV^{-1}C_n^2[(f/V)^2 + (1/2\pi L_0)^2]^{-4/3} \quad 0 < f < V/l_0 \quad [\text{rad}^2/\text{Hz}], \quad (5)$$

exhibiting a spectrally flat behavior at frequencies below  $V/L_0$ . Finally, the Greenwood-Tarazano spectrum yields [38]

$$S_\phi(f) = 0.0097k^2C_n^2LV^{-1} \int_{-\infty}^{\infty} [(f/V)^2 + q_y^2 + \sqrt{(q_y^2 + (f/V)^2/(2\pi L_0)^2)}]^{-11/6} dq_y, \quad (6)$$

which also flattens at frequencies below  $V/L_0$ . These equations ignore aperture averaging and the subtleties associated with a Gaussian beam versus a plane or spherical wave, but the basic scaling for the phase PSD remains the same below Fourier frequencies associated with the aperture diameter [3,4,36,39,42]. Therefore, in principle, examination of the low-frequency component of the phase PSD can provide insight into the presence of an outer scale.

All experimental results will be quoted in the timing-jitter PSD that can be related to the phase PSD by  $S_{\text{jitter}}(f) = (2\pi\nu_0)^{-2}S_\phi(f)$ .  $S_{\text{jitter}}(f)$  is plotted in Fig. 1 for Eqs. (4)–(6). There can be higher-order turbulence-induced dispersion that will further increase the timing jitter on the pulses, but for the picosecond pulse lengths and kilometer-scale path lengths used here, these effects are negligible [1,13,43]. In other words, the dominant effect is fluctuations in the pulse-to-pulse arrival time from the path-averaged index of refraction variations rather than intrapulse temporal broadening.

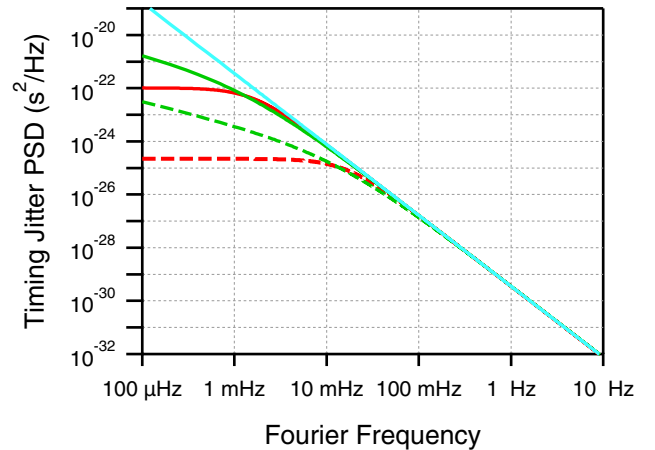


FIG. 1. (Color online) Theoretical predictions for the timing-jitter power spectral density (PSD). The PSDs calculated from the Kolmogorov spectrum, light blue (light gray), von Karman spectrum, red (dark gray), and Greenwood-Tarazano spectrum, green (medium gray), are shown for  $V = 1 \text{ m/s}$ ,  $C_n^2 = 10^{-14} \text{ m}^{-2/3}$ , and  $L = 2 \text{ km}$  with an outer scale of either  $L_0 = 10 \text{ m}$ , dashed lines, or  $L_0 = 100 \text{ m}$ , solid lines, for the von Karman and Greenwood-Tarazano spectra. Note that all show an  $f^{-8/3}$  scaling for Fourier frequencies above  $\sim 20 \text{ mHz}$ .

The angle-of-arrival fluctuations,  $\alpha(t)$ , are driven by the spatial derivative of the optical phase across the wave front, and therefore are closely related to the optical phase noise PSD through [3,39]

$$S_\alpha(f) = (2\pi c/V)^2 f^2 S_{\text{jitter}}(f), \quad (7)$$

with an additional roll-off at higher frequencies due to aperture averaging. This scaling arises from the direction connection between  $\alpha(t)$  and the spatial derivative of  $\varphi$ . Its derivation requires Taylor's hypothesis but is independent of the turbulence spectrum.

### III. EXPERIMENTAL SETUP

Previous laser-based measurements of the atmospheric phase noise have been made through cw laser heterodyne interferometry. (See Sec. IV.) This approach can be quite sensitive, as an easily measured  $2\pi$  optical phase change corresponds to  $\sim 5$  fs of timing jitter at 1550 nm. However, especially over longer, turbulent paths, signal fading will lead to slips in the detected phase [14,44] and therefore will accumulate 5-fs ambiguities. As a result, it is difficult to acquire continuous phase measurements over long periods. Note that the frequency variation, which is the derivative of the phase variation, can still be obtained as in Ref. [14] to yield the frequency noise PSD. We have conducted cw laser heterodyne measurements over a 2-km horizontal path using a state-of-the-art free-space optical terminal. We find the maximum phase-slip free period is only tens of seconds for our typically turbulent conditions, so it is not possible to measure the optical phase PSD reliably below 100 mHz. Furthermore, the presence of phase slips leads to unpredictable distortions of the PSD depending on the duration and spacing of the phase dropouts. For short time scales without phase slips, good agreement is seen, as demonstrated in Sec. IVB in the comparison between the group delay and carrier-phase delay.

Here we rely primarily instead on a frequency-comb-based approach. In the time domain, our frequency-comb source emits a series of optical pulses whose timing is coherently phase locked to an underlying optical reference. For our 100-MHz repetition rate comb, these pulses are separated by 10 ns. We transmit these pulses over a free-space path and measure the change in their arrival time. Rather than utilize direct photodetection of the pulse arrival time, which would severely limit the timing precision, we detect the arrival time with femtosecond-level precision through coherent linear optical sampling (LOS) with a second frequency comb, as described below and in Ref. [45]. With this approach, unlike the case of a cw laser heterodyne measurement, there is no loss of timing information across time periods with strong signal fading. Consequently phase fluctuations can be continuously measured over very long time periods across a long turbulent path.

A simplified schematic is shown in Fig. 2 and described in more detail in Ref. [6]. Both combs are phase locked to the same underlying optical reference cavity via two cw reference lasers. The net effect is that the relative pulse timing between the two combs is known precisely to femtosecond levels, and likewise their relative carrier phase is known to less than a radian. The coherent pulse train from one comb (blue in Fig. 2) is filtered to an optical bandwidth of  $\sim 1$  THz (7 nm) centered

at 1553 nm and average power of 2 mW. It is then launched into single-mode optical fiber to a room at the top of the NIST building in Boulder, Colorado. From there, the pulses are launched from a free-space terminal with a 5-cm aperture diameter across the air path to a mirror on a hill 1 km distant and back to a free-space terminal in a second room, where the light is collected in a single-mode fiber and transmitted back to the laboratory. [See Fig. 2(a).] The total fiber-optic path length, including a 120-m spool of dispersion-compensating fiber in the laboratory, is  $\sim 500$  m. The received power varied from 20  $\mu$ W down to a minimum detectable power of 70 nW, corresponding to a 20–44-dB link loss [6]. Fast-steering mirrors on both sides of the link compensated for beam wander via a dither lock with a  $\sim 200$ -Hz bandwidth. The mirror correction signals were digitized and recorded to evaluate the angle-of-arrival jitter,  $\alpha(t)$ .

Fluctuations in the optical path length lead to fluctuations in both the pulse timing and carrier phase. These path-length fluctuations can arise from changes in the optical-fiber length or in the air path. To detect these fluctuations, the received signal is heterodyned against the second comb [labeled red in Fig. 2(b)]. This comb has its repetition rate purposefully offset by exactly  $\Delta f_r$  so that its pulses “walk through” the incoming pulse train; the result is a series of interferograms, or cross correlations, which occur every  $1/\Delta f_r$  (or 318  $\mu$ s in our case) as shown in Fig. 2(c). Any variation in the time of flight of the received pulses,  $\Delta x_{\text{group}}$ , appears as a much larger variation in the spacing of the interferograms,  $(f_r/\Delta f_r)\Delta x_{\text{group}}$ . (The system is exactly analogous to a sampling oscilloscope.) In addition, any variation in the carrier phase of the received pulses,  $\Delta\phi$ , is recorded in the phase of the interferogram oscillations and has a corresponding time delay of  $\Delta x_{\text{phase}} = \Delta\phi/(2\pi\nu_0)$ . Both the group delay,  $\Delta x_{\text{group}}$ , and the carrier-phase delay,  $\Delta x_{\text{phase}}$ , are extracted from the measured interferograms through spectral-domain-based processing as described in more detail in the Supplemental Material of Ref. [20]. For propagation through air, they are nearly equal, with  $\Delta x_{\text{group}} \approx \Delta x_{\text{phase}}$  to within a factor of  $(1 - n_{\text{group}}/n_{\text{phase}})$ . However, the group delay measurement is much more robust to scintillation and other signal-fading effects, since it has an effective ambiguity of 10 ns as compared to the ambiguity of 5 fs associated with the carrier-phase measurements.

Based on the angle-of-arrival variations, we estimate  $C_n^2$  varied between  $10^{-15}$  and  $10^{-14}$   $\text{m}^{-2/3}$  over these measurements. For the carrier wavelength of 1553 nm, the Rytov variance is below the weak-turbulence limit of 0.3 for path lengths up to 1 km [1]. Therefore, at the round-trip path length of 2 km, some deviation from the weak-turbulence limit could be expected for amplitude measurements. However, phase-noise-related turbulence phenomena have been shown to agree quite well with predictions for the weak-turbulence limit even at larger Rytov variance [1]. As we focus here on phase effects rather than amplitude effects such as scintillation, we expect not to see deviations from the weak-turbulence limit.

The 15 measurements discussed in Sec. IV were taken over the span of a week in August with start times ranging from 7:00 am to 10:30 pm with each measurement period ranging from a 1-h to 3.7-h duration. Measurement periods included both clear skies as well as overcast skies with an

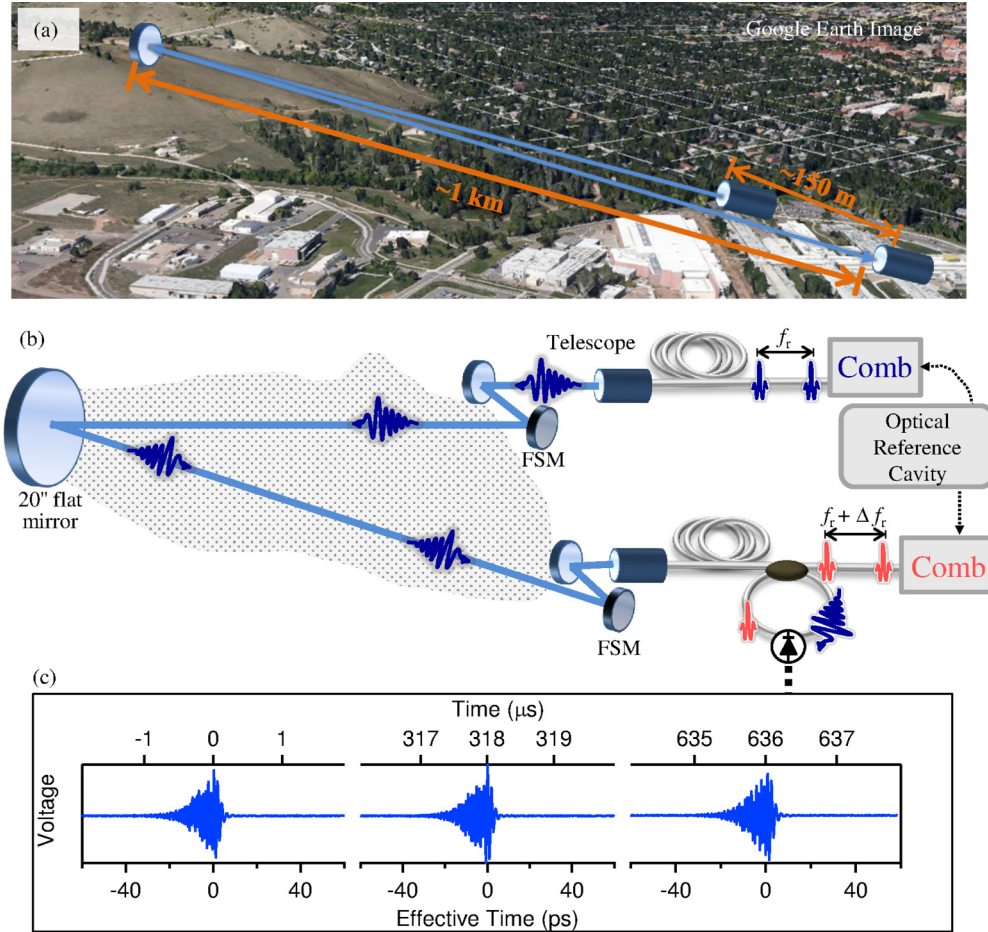


FIG. 2. (Color online) Experimental setup. (a) Image of 2-km round-trip air path with locations of the mirror, beam-launching, and beam-catching telescopes. The air-path elevation varied from 3 m, across the building roof, to 100 m above a surface consisting mostly of grass and trees, but also with short sections of asphalt and the building roof. Over the air path, the return beam from the mirror does not overlap with the outgoing beam. (b) A frequency comb generates a coherent pulse train at a repetition rate,  $f_r$ , blue (dark gray) pulses, centered at 1553 nm, which traverses the air path, blue (dark gray) lines, as well as  $\sim 500$  m of single-mode optical fiber, light gray lines. A second frequency comb, red (light gray) pulses, at a repetition rate,  $f_r + \Delta f_r$ , and stabilized by a common optical reference is used for LOS detection of the incoming pulse train with femtosecond-level timing. Fast-steering mirrors (FSM) on either side of the air path compensate for beam wander. Environmental variables including temperature, humidity, pressure, and wind speed were recorded near the beam-launch location as well as at the 20-in. flat mirror on the hill. (c) LOS of the incoming comb pulses with an asynchronous second comb returns an interferogram every 318  $\mu\text{s}$  ( $1/\Delta f_r$ ) in real (lab) time. At each of these points the down-sampling nature of LOS provides ultrahigh-resolution “effective time” measurement of time-of-flight variations around the expected arrival time [6,45].

air temperature ranging from 15 °C to 35 °C. For all the measurements, wind speeds were light and variable with typical wind speeds of 1–2 m/s.

#### IV. RESULTS

##### A. Timing jitter measured by the frequency-comb-pulse time-of-flight variations

The coherence of the frequency combs enabled measurements over hours, far exceeding the time scale set by  $L_0/V$ , i.e., tens to hundreds of seconds for different estimates of  $L_0 \sim 10$ –100 meters [3,9,35,41] and the measured wind speeds of  $V \sim 1$ –2 m/s. Over these long time scales, optical path-length changes are a result not of turbulence, but simply of environmental variations. In particular, the effective path length in air will change by  $-0.75$  ppm/°C with temperature

and by 2.7 ppb/Pa with pressure [40]. Figure 3 compares the measured fractional change in optical path length with the expected fractional change from the recorded temperature and pressure values. The slight quantitative disagreement partly reflects the nonuniform air path and the point-measurement nature of the weather sensors. In addition, the fiber paths that connect the frequency combs to the free-space terminals undergo both vibrations and temperature cycling (from the air conditioning). The former leads to higher frequency noise in the PSD, discussed later. The latter leads to  $\sim 10$ –15-min oscillations in the fiber path length that can, in some cases, approach a picosecond delay.

The time-of-flight fluctuations are analyzed for each measurement in terms of the power spectral density (PSD). Figure 4 shows a PSD of the timing jitter,  $S_{\text{jitter}}(f)$ , across the entire path comprising both the 2-km air path and  $\sim 500$ -m fiber path

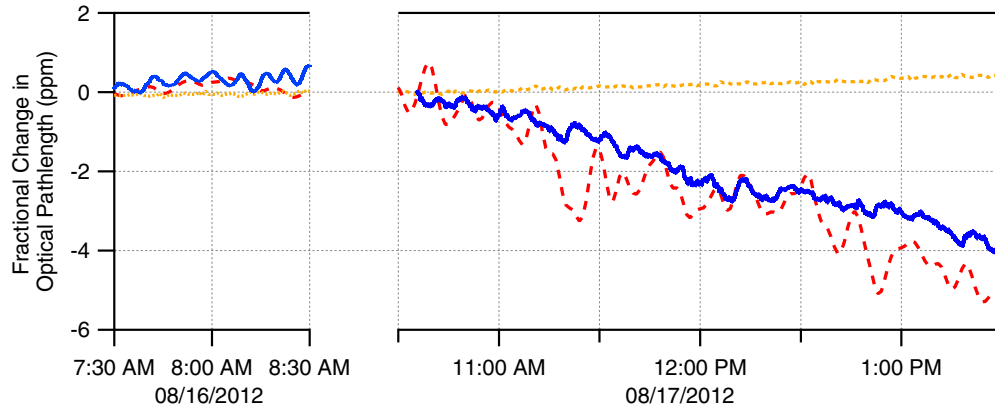


FIG. 3. (Color online) Long-time-scale fluctuations. Data from both stable atmospheric conditions (left) and a period of changing temperature (right) showing measured fractional change in optical path length, solid blue (dark gray) line, as well as the expected contributions due to measured change in temperature, dashed red (dark gray) line, and pressure, dashed orange (light gray) line. The cumulative fractional optical path length change of  $\sim 4$  ppm from the period of changing temperature corresponds to a 27-ps differential delay. The  $\sim 10$ -min oscillations strongly evident on the left-hand side are a result of air-conditioning cycles affecting a fiber-optic spool length in the laboratory, as discussed in the text. The data presented on the right was previously shown in Ref. [6] and is included here as it most clearly demonstrates the impact of a period of changing temperature.

from a 3.7-h data run. The contribution from fiber path-length fluctuations is quantified by two additional PSDs in Fig. 4. The first (light blue line) is a measure of the time-of-flight variations from the 380-m fiber path through the building that connects the laboratory with the free-space launch sites and which is subjected to vibrations, resulting in the noise increase at tens of Hz. The second (orange line) is a measure of the time-of-flight variations for a  $\sim 120$ -m dispersion-compensating spool that was part of the fiber path but located in the laboratory, where there was significant temperature cycling. This fiber led to the 10–15-min temperature cycling evident in Fig. 3 and in the peak of the PSD at 2 mHz. As the amplitude of this peak depends on the intensity of the temperature cycling, in some cases, a corresponding peak is visible in the total PSD, but otherwise the fiber path contribution to the noise is significantly below the air-path contribution for frequencies below 10 Hz. Above 10 Hz the fiber noise obscures

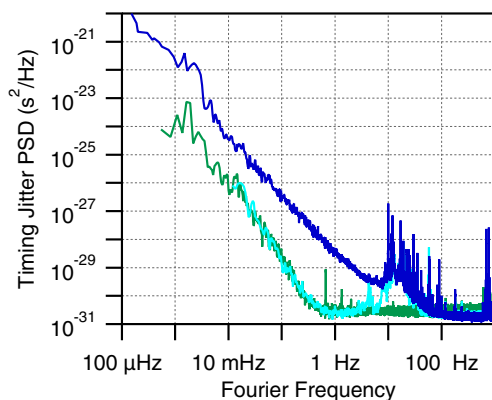


FIG. 4. (Color online) Power spectral density of timing jitter,  $S_{\text{jitter}}(f)$ , in the pulse time of flight across the entire path comprising 2 km of air and 500 m of fiber from 100  $\mu\text{Hz}$  to 1 kHz, dark blue (dark gray), as well as the contribution only from the 500 m of fiber path from building vibration-induced noise, light blue (light gray), and laboratory temperature cycling, green (medium gray).

the turbulence contribution including the impact of aperture averaging and any inner scale. Finally, note that the intrinsic system noise is negligible (below  $1 \text{ fs}^2/\text{Hz}$  [6]), and in the future the fiber-path contribution could be eliminated through the use of frequency combs located at the launch site.

Figure 5 shows four timing-jitter PSDs,  $S_{\text{jitter}}(f)$ , (dark blue) for  $f < 1$  Hz, where the atmospheric effects dominate. Following Eq. (4), the PSD is fit to  $\log[S_{\text{jitter}}(f)] = \log[Af^{-\gamma}]$  with a linear frequency point spacing, where the constant  $A$  depends on the wind speed and  $C_n^2$ , and the scaling exponent  $\gamma$  is expected to be  $\gamma = 8/3 = 2.67$  from Sec. II. The PSDs were fit between 4 and 500 mHz to avoid contributions from fiber noise, which is 10–20 dB below the measured data over this range. The fits return a power-law scaling of  $\gamma = 2.39, 2.09, 2.33,$  and  $2.40$  (red line) for Figs. 5(a)–5(d), respectively. This scaling difference between the measured values and the expected value of 2.67 is not particularly compelling for a single data set; it would be easy to assign a  $-8/3$  slope, as was done in Ref. [6]. However, as shown in Fig. 6(a), fits of 15 PSDs acquired with measurement durations from 1 to 3.7 h consistently return a scaling law shallower than the predicted Kolmogorov scaling. Interestingly, the average scaling exponent was  $\langle \gamma \rangle = 2.31 \pm 0.14$ , which lies between the Kolmogorov  $f^{-8/3}$  scaling and the  $f^{-2}$  scaling of a random walk.

Interestingly, the data in Fig. 5 show no strong evidence of a roll-off in the PSDs at low Fourier frequencies, although there is significant scatter. Figure 6(b) shows the average of these PSDs, which reduces the scatter at very low Fourier frequencies. The PSD of Fig. 6(b) exhibits no roll-off, even down to very low Fourier frequencies of 100  $\mu\text{Hz}$ . For a typical wind speed of  $V \sim 1$  m/s, a roll-off beginning at 100  $\mu\text{Hz}$  would correspond to an outer scale of 10 km, which is clearly unphysical [9,35,41].

### B. Timing jitter from the comb's carrier-phase variations

As discussed in Sec. III, the measurement system can retrieve both the variations in the group delay (or time-of-flight of

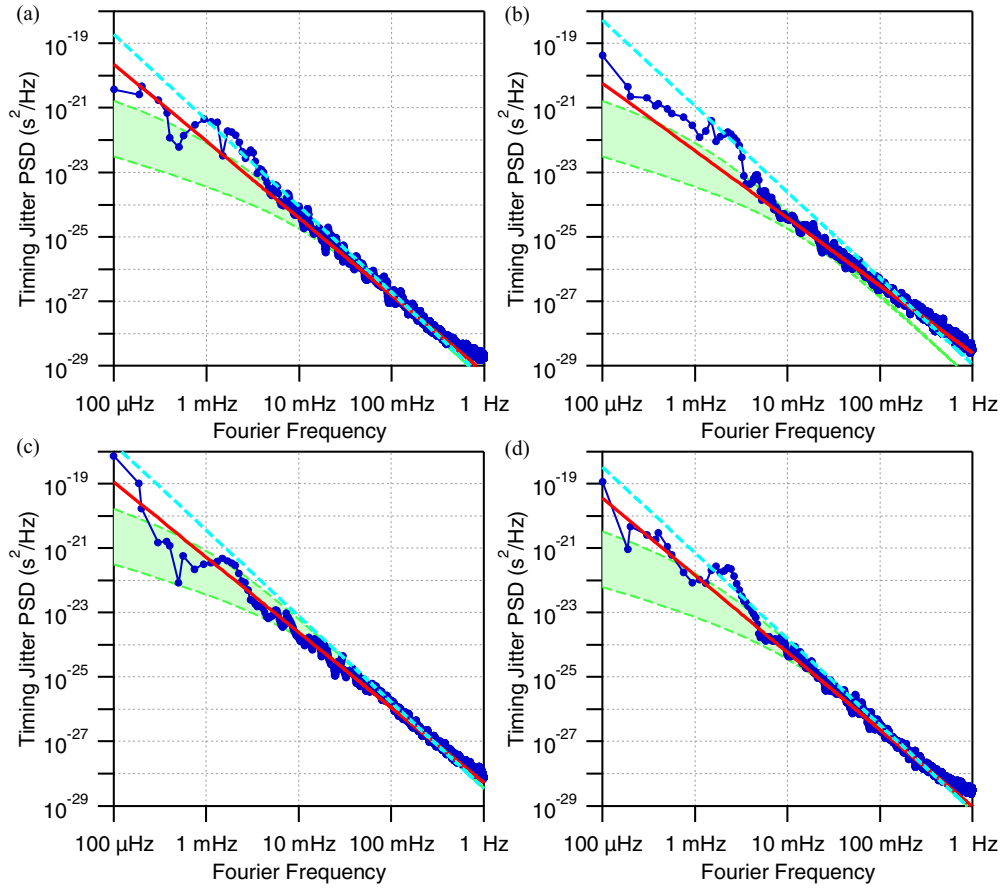


FIG. 5. (Color online) Four timing-jitter PSDs, dark blue (dark gray) circles, and a fit, red (solid dark gray) line, to a single power-law scaling with exponents of 2.39, 2.09, 2.33, and 2.40 for the (a)–(d) PSDs, respectively. In addition, the plots show for comparison, a PSD with the expected Kolmogorov power-law scaling of  $8/3$ , dashed light blue (light gray) line, and the range of PSDs for the Greenwood-Tarazano spectrum, shaded region, with an outer scale of  $L_0$  between a lower bound of 10 m and an upper bound of 100 m. The PSD shows no significant sign of flattening down to 100  $\mu\text{Hz}$ . The integrated timing jitter from 100  $\mu\text{Hz}$  to 1 kHz is  $\sim 1, 3, 13,$  and 6 ps for (a)–(d), respectively.

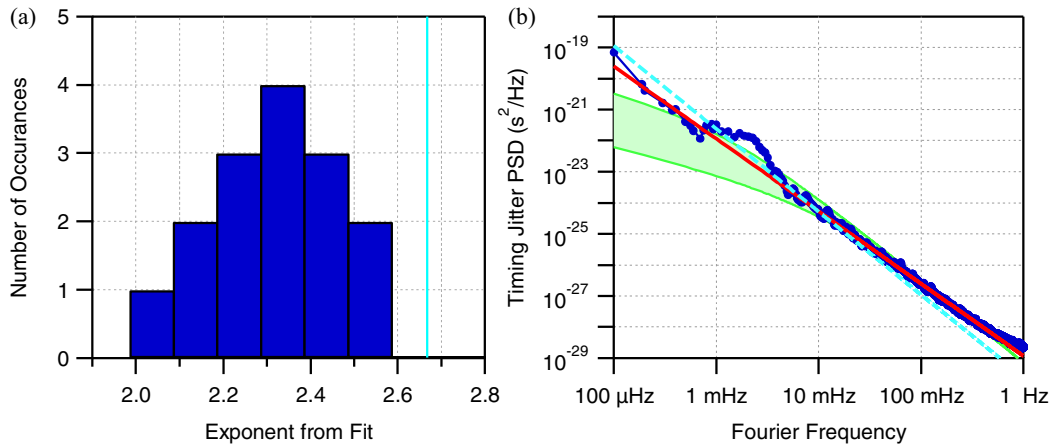


FIG. 6. (Color online) (a) Histogram of power-law scaling exponent,  $\gamma$ , from a fit to  $S_{\text{jitter}}(f) \sim f^{-\gamma}$  for 15 measurements ranging from 1 to 3.7 h. The light blue (light gray) line marks the expected  $\gamma = 8/3 \approx 2.67$  Kolmogorov scaling. The average value of the exponent is instead  $\gamma = 2.31 \pm 0.14$ . (b) Average PSD from the data of Fig. 5 demonstrating the single power-law scaling. The red (solid gray) line is a fit to the average PSD over a range of 4 to 500 mHz, which returns an exponent of  $\gamma = 2.33$  instead of the expected  $\gamma = 8/3 \approx 2.67$  Kolmogorov scaling, light blue (light gray) dashed line, or the Greenwood-Tarazano spectrum shown for outer scales,  $L_0$ , between 10 and 100 m, shaded region. The pronounced hump around 2 mHz is due to the building-temperature-cycling-induced fiber noise.

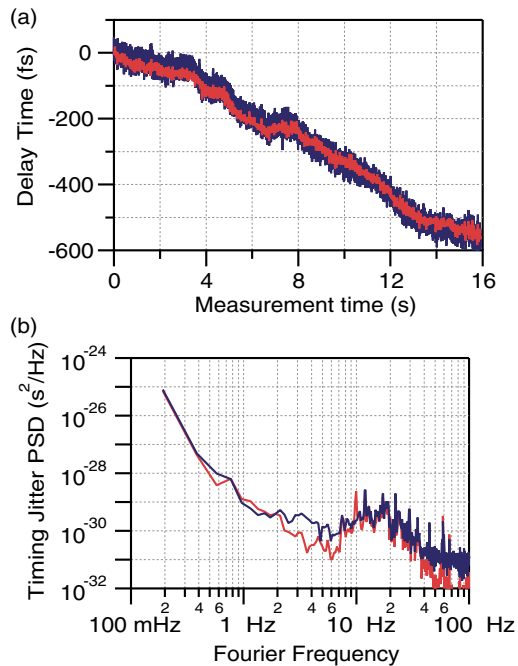


FIG. 7. (Color online) (a) Comparison of the group delay, blue (dark gray), and carrier-phase delay, red (light gray), for a low-turbulence period with few, or no, carrier-phase phase slips. (b) Corresponding PSD for the group and carrier delays. The increase below 10 Hz is due to variations in the fiber-optic path length, as in Fig. 4.

the pulses) and the carrier-phase delay of the transmitted comb pulse train. For most turbulence conditions, the carrier phase is an unreliable metric of the total phase jitter since  $2\pi$  phase slips are undetected between interferogram measurements that are spaced by  $\Delta f_r \approx 300$  us and even longer dropout periods are often observed due to scintillation. However, for quiet periods and if the occasional phase slip is not critical, the carrier phase can have much lower noise than the group delay measured through the pulse time-of-flight. Figure 7 compares the carrier-phase delay and group pulse delay over such a quiet period. The two agree well and the slight difference in accumulated delay can be attributed to the difference in  $C_n^2$  due to the difference between the group and phase indices of refraction.

The correspondence between the group and phase delays assumes that the turbulence effects are fully correlated across the  $\sim 1$ -THz optical-frequency bandwidth of the pulses. If, instead, there is a decorrelation of turbulence phase noise with optical frequency, the pulses can experience additional time variations. Several authors have explored the magnitude of this intrapulse effect, or turbulence-induced dispersion, and found it to be much smaller than the direct pulse-to-pulse timing jitter [1,13,43]. Its effect would appear here as a time-varying coefficient to a quadratic fit of the spectral phase. In fits to our data before the spectral-domain processing to extract the delay, we see no quadratic term at the level of  $8 \times 10^{-26}$  s<sup>2</sup>, consistent with the prediction for the 2-km path length and  $\sim 1$ -THz bandwidth [1].

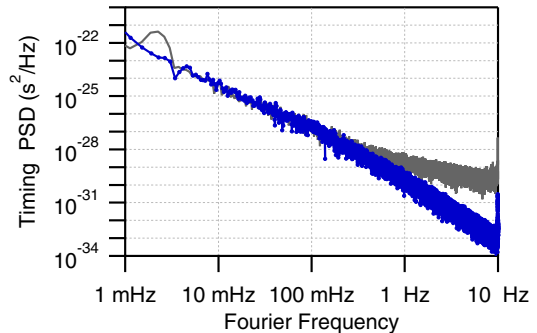


FIG. 8. (Color online) Angle-of-arrival PSD scaled as  $(2\pi cf/V)^{-2}S_\alpha(f)$ , blue (dark gray) line, with  $V = 0.7$  m/s. From Eq. (2.7), this scaled PSD should overlap the time-of-flight PSD, light gray line, which it does, except where the fiber-path noise dominates at 2 mHz and above 0.5 Hz.

### C. Timing jitter from the scaled angle-of-arrival PSD

The angle-of-arrival fluctuations can be extracted from the mirror correction signal (see Fig. 2) for Fourier frequencies below the feedback bandwidth of  $\sim 200$  Hz. Following Eq. (7), the angle-of-arrival PSD,  $S_\alpha(f)$ , is simply a scaled version of the time-of-flight PSD,  $S_{\text{jitter}}(f)$ . Figure 8 compares the appropriately scaled  $S_\alpha(f)$  to  $S_{\text{jitter}}(f)$  for one data run. The agreement is excellent; as expected, angle-of-arrival PSD shows no contribution from the fiber-path noise (Fig. 4), but otherwise tracks the timing-jitter PSD perfectly. From these data, we can extend the  $7/3$  power-law scaling observed in  $S_{\text{jitter}}(f)$  out beyond 1 Hz, but with the caveat that such an extension relies on “perfect” cancellation of the true angle-of-arrival jitter by the feedback system.

Experimentally, the fast-steering mirror could introduce a “piston”-like motion that is correlated with the angular deviation, unless the laser beam is perfectly aligned with the rotation axis of the mirror. The piston noise would appear as path-length variation indistinguishable from the atmospheric phase variation, except with a power-law scaling that differs by  $f^2$  [see Eq. (7)]. From our data, this coupling is estimated to be below  $0.2$  fs/ $\mu$ rad, which should lead to a negligible contamination of  $S_{\text{jitter}}(f)$  below 10 Hz.

## V. DISCUSSION

### A. Comparison with predictions

From an empirical point of view, the results are simple. The optical phase PSD follows a single power-law scaling of  $S_\phi(f) \propto f^{-7/3}$  from  $100$   $\mu$ Hz out to  $0.5$  Hz, based on the pulse measurements, and out to  $10$  Hz if extended through the angle-of-arrival measurements. This scaling covers up to five orders of magnitude in frequency with no roll-off at low Fourier frequencies, due to an outer length scale.

This simple power law is surprising in the context of standard turbulence theory outlined in Sec. II, where an assumed spatial scaling of the turbulence is mapped to the frequency domain through Taylor’s frozen-turbulence hypothesis. In this picture, the optical phase PSD would exhibit four distinct regions: (1) a very steep roll-off at high frequencies,  $f > V/l_0$ , corresponding to the dissipative region (or actually sooner due

TABLE I. Comparison of experimental results on atmospheric optical phase noise power spectral density.

Reference	Experimental configuration	Path length	Fourier frequency range	Deviation from Kolmogorov scaling	Outer scale
[8]	Laser interferometer <sup>a</sup> at 632 nm	50 m	1 Hz–300 Hz	−0.17	~1 m
[9]	Dual-beam laser interferometer	70 m	200 mHz–500 Hz	0	No evidence <sup>b</sup>
[11]	Dual-beam laser interferometer at 632 nm	100 m	100 mHz–200 Hz	0	No evidence <sup>c</sup>
[20]	Laser interferometer at 632 nm	11 m	100 mHz–100 Hz	−0.2	None (requires $L_0 > 11$ m)
[20]	Stellar interferometry	NA	10 mHz–5 Hz	−0.43	Tens of meters
[12]	Stellar interferometry	NA	1 mHz–100 Hz	−0.12	No evidence
[19]	Stellar interferometry	NA	1 mHz–100 Hz	None reported	No evidence
[15]	Stellar interferometry	NA	100 mHz–1 Hz	−0.2 to −0.3	Tens of meters
[14]	Laser interferometer at 1000 nm	5 km	1 mHz–10 Hz	−0.4	No evidence below a few km
[44]	Laser interferometer at 1500 nm	4 and 35 km	5 mHz–50 Hz	0	Some indication <10 mHz ( $L_0 \sim 100$ 's of meters)
This work	Comb pulses at 1550 nm	2 km	100 $\mu$ Hz–1 Hz	−0.36	None

<sup>a</sup>The structure function was directly measured over a given time range. If it scales as  $\langle D(t)D(t + \tau) \rangle \sim \tau^{\gamma-1}$ , then the corresponding PSD scales as  $S_{\Delta\phi}(f) \sim f^{-\gamma}$  [10].

<sup>b</sup>There was evidence of an outer scale in the spatial structure function but not in the PSDs.

<sup>c</sup>Any roll-off is indistinguishable from filtering effects.

to aperture averaging); (2) a “Kolmogorov”  $f^{-8/3}$  scaling over the frequency range  $V/L_0 < f < V/l_0$ , corresponding to the inertial region; (3) a flat  $f^0$  scaling at low frequencies,  $f < V/L_0$ , corresponding to the energy-input spectral region; and (4) an  $f^{-n}$  scaling at very low frequencies,  $f < V/L$ , corresponding to changes in air temperature (weather). Instead, the observed optical phase PSD follows the much simpler  $f^{-2.3}$  scaling across *all* frequencies from 0.5 Hz to 100  $\mu$ Hz, which easily cover the last three frequency regions; in other words, the PSD consistently follows a scaling that lies between the Kolmogorov  $f^{-8/3}$  scaling and a random-walk  $f^{-2}$  scaling, with no evidence of an outer scale, distinct input spectral region, or distinct weather-related region.

Perhaps this disagreement is not surprising in light of the strong assumptions made in Sec. II [2,35]. Certainly the simple “8/3” Kolmogorov scaling in the inertial region cannot capture the full complexity of the outdoor wind patterns, thermal sources, and path obstructions [12]. Furthermore, beyond the inertial region, measurements of the microtemperature fluctuations such as those in Ref. [38] indicate a gradual roll-off in the PSD in the input spectral region as captured by the Greenwood-Tarazano spectrum [18,38]. However, even this more gradual roll-off, plotted in Fig. 1, is not observed as shown in Fig. 6(b). Most importantly, Taylor’s hypothesis will almost certainly not be valid at time scales beyond 0.1 to a few seconds, depending on the eddy size [18,35,46] (in particular, see Appendix B2 of Ref. [18]). The overall frequency dependence must be a result of both the translation effects of wind and the intrinsic time-dependent evolution of the turbulent eddies.

## B. Comparison with previous results

Indeed, while some experiments have confirmed the Kolmogorov  $f^{-8/3}$  scaling, a number of experiments have also found shallower power-law scaling for Fourier frequencies as low as 1 mHz [8,9,11,12,14,15,20,44]. In our work, we have extended the range of Fourier frequencies probed down to 100  $\mu$ Hz. Furthermore, the evidence in the literature for an outer scale in the PSD is mixed. Table I is a partial summary of past work listing the experimental configuration, path length, Fourier frequency range, power-law scaling deviation from the Kolmogorov scaling given in Sec. II for  $S_\phi(f)$  or  $S_{\Delta\phi}(f)$  (i.e., deviation =  $\gamma - 8/3$  in the inertial region), and outer scale estimate. Experiments fall into two classes. In laser heterodyne experiments, researchers probe the optical phase PSD along a single horizontal path,  $S_\phi(f)$  or the optical phase difference (structure function) PSD between two parallel horizontal paths,  $S_{\Delta\phi}(f)$ . In stellar interferometry experiments, the optical phase difference between two parallel vertical paths,  $S_{\Delta\phi}(f)$ , is recorded via the required control signal applied to the optical delay line connecting the displaced telescope receivers. Some quantities are only roughly estimated from available figures, and there are many subtleties clearly elucidated in the references but not captured in the table. While there is strong variability in the table, the Kolmogorov scaling is often not observed. (Although not included, the PSD at 5 GHz carrier acquired with the Very Large Array also exhibits a shallow power scaling of  $\gamma = 2.4$  [10]). Moreover, the evidence for an outer scale in the PSDs (which would appear as a roll-off at low Fourier frequencies) is often absent. In many cases, the last few data points in the PSD can indicate a slight roll-off, but these last points

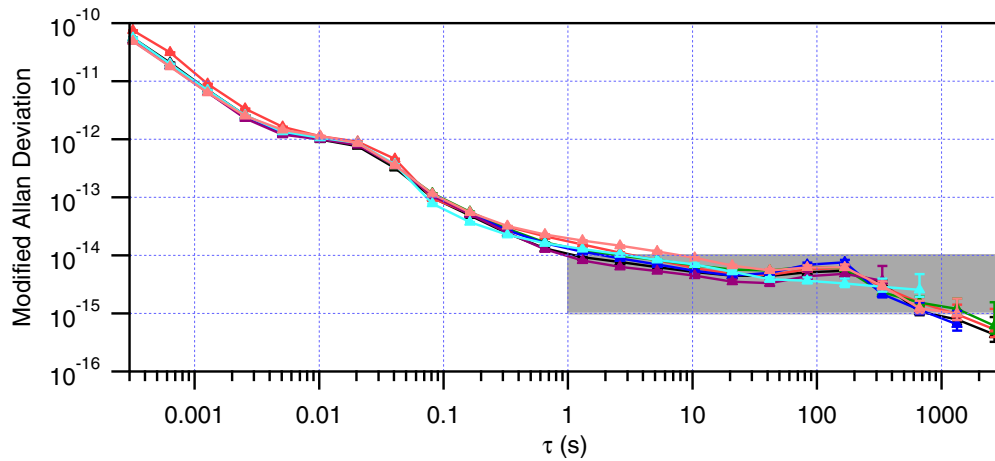


FIG. 9. (Color online) Modified Allan deviation. Multiple measurements are shown for the 2-km path to show the similarity between measurements (triangles). The shaded region represents the limit set on the accuracy by temperature drifts of 0.5 to 5 °C/h or platform motion of 1 mm/h to 1 cm/h.

are notoriously noisy. By probing to much lower Fourier frequencies, our data dispel the notion that the outer scale lurks just below the  $\sim 10$  mHz range. Furthermore, since our data have no hidden phase slips, the power-law response is uncontaminated by potential systematics and the observed shallow power-law response can be fully attributed to the atmosphere. Finally, note that the absence of a low-frequency roll-off in the PSDs does not preclude the existence of an outer scale, and a number of the referenced works do find an outer scale in the spatial structure. The absence of the roll-off in the PSD simply indicates a breakdown in Taylor's hypothesis at low Fourier frequencies (long time scales).

### C. Implications for stability and accuracy of one-way optical time-frequency transfer

The impact of atmospheric turbulence on the stability and accuracy of one-way optical time-frequency transfer is significant [6,14,21]. The same data that yield the optical phase noise PSD can be used to calculate the timing stability for the one-way time of flight, as characterized by the modified Allan deviation. As shown in Fig. 9, at short time scales (high Fourier frequencies), shot noise, comb jitter, and fiber path-length variations dominate the stability, but beyond a few seconds the turbulence noise leads to a flickerlike floor. For the measured power-law scaling of  $f^{-2.3}$ , the modified Allan deviation falls only as  $\sim \tau^{-1/3}$  [14,47]. Therefore although a stability of  $10^{-13}$  is already reached at 0.1 s, it takes an additional 1000 s to reach  $10^{-15}$  due to atmospheric turbulence.

A low stability is of little meaning if there is a larger systematic bias. A linear temperature gradient of  $dT/dt$  will cause such a bias, leading to a fractional inaccuracy of  $\sim 10^{-6}(L/c)(dT/dt)$  because of the  $\sim 1$  ppm/°C change in the air index of refraction. Over  $L = 2$  km, temperature gradients of 0.5 to 5 °C/h limit the accuracy to  $10^{-15}$ – $10^{-14}$  (e.g., the data of Fig. 3 have a systematic bias of 2.7 ps/3 h =  $2.5 \times 10^{-15}$ .) This bias will not appear in the stability plot unless  $\tau$  extends over many days and it will grow with longer atmospheric paths. Likewise, any relative platform motion will limit the accuracy through the Doppler shift. A relative velocity of 1 mm/h to 1 cm/h similarly limits the accuracy

to  $10^{-15}$  to  $10^{-14}$ . Therefore, the accuracy limitations to any long-path one-way optical-frequency transfer are potentially even more problematic than the instability limits from atmospheric turbulence.

This systematic bias could, in principle, be removed through careful measurement of the temperature and platform velocity. However, such measurements are challenging and for longer paths, the requirements for removing the temperature drift become even more critical. A more effective solution to this challenge is provided by the reciprocity of a single-mode link through the atmosphere. The atmosphere has been shown both theoretically [48–51] and through measurements of amplitude fluctuations [51,52] to be reciprocal for propagation times shorter than the coherence time of the turbulence. In Ref. [6], we demonstrated that the time-of-flight fluctuations could be canceled through the use of a two-way single-mode link achieving stabilities below  $10^{-18}$  at 1000 s and a systematic bias below  $4 \times 10^{-19}$ . A similar reciprocity-based solution does not exist for stellar interferometry or laser ranging.

## VI. CONCLUSIONS

Frequency-comb pulses were transmitted across a 2-km turbulent air path and detected via heterodyne mixing against a second, coherent frequency comb. This technique can record the variations in pulse arrival time over very long time periods, and therefore the evaluation of the atmospheric phase noise PSD at much lower Fourier frequencies than is possible with a conventional cw laser heterodyne measurement. From an empirical point of view, the results are straightforward: The optical phase PSD follows a single power-law scaling of  $f^{-2.3}$  from 100  $\mu$ Hz out to 0.5 Hz, based on the pulse measurements, and out to at least 10 Hz if extended through the angle-of-arrival measurements. This scaling covers five orders of magnitude in frequency with no roll-off at low Fourier frequencies due to an outer length scale.

This measured atmospheric phase noise has implications for one-way optical time-frequency transfer. The corresponding instability or precision, as characterized by the modified Allan deviation, is only  $10^{-14}$  to  $10^{-15}$  from 1- to 1000-s

observation periods even at modest turbulence levels of  $C_n^2 \sim 10^{-14}$ – $10^{-15}$  and relatively short path length of 2 km. This level of instability is insufficient to support state-of-the-art optical clocks [53–56]. Additionally, systematic bias from air temperature gradients or platform motion will also limit the accuracy in any one-way link.

The results presented here contrast with predictions based on the expected spatial power spectrum of turbulent eddies and Taylor’s frozen-turbulence hypothesis. Over the frequency range observed here, one might expect at least three distinct regions for the slope in  $S_\phi(f)$ : (i) a Kolmogorov-like  $f^{-8/3}$  scaling across the inertial region, (ii) an almost flat PSD across the input energy region where wind shear or convection causes large eddies, and (iii) yet a different scaling to capture the gross air temperature and pressure changes. None of these transitions are observed, but instead  $S_\phi(f)$  follows a simple power law with no roll-off at low frequencies, consistent with other examples in the literature albeit measured to lower Fourier frequencies. The possible explanations include [10,12,15,18–20,46,57] invalidity of the Taylor frozen-turbulence hypothesis, intermittent turbulence, variations in

wind speed, turbulent layers, and obstructions. The lack of a roll-off at low Fourier frequencies does not preclude the existence of an outer scale in the spatial turbulence spectrum; it is simply that this outer scale is not mapped directly to the optical PSD through the wind speed. The quantitative disagreement between the measurements and theory is perhaps not surprising given the complexity of a real world link. Regardless of the explanation, the shallower-than-expected scaling of the optical phase PSD in the inertial region and the continued growth of the optical phase noise at very low frequencies has consequences for any measurement that requires long integration times such as precision stellar interferometry, optical time-frequency transfer, and laser ranging.

#### ACKNOWLEDGMENTS

We acknowledge funding from the DARPA PULSE and QuASAR programs and helpful comments from J. D. Deschenes, R. Hui, and E. Williams. Work of the US government, not subject to copyright.

- 
- [1] R. L. Fante, *Proc. IEEE* **63**, 1669 (1975).
- [2] A. Ishimaru, *Wave Propagation and Scattering in Random Media* (Academic Press, New York, NY, 1978).
- [3] F. Roddier, in *Progress in Optics*, edited by E. Wolf (North-Holland, Amsterdam, 1981), pp. 281–376.
- [4] L. C. Andrews and R. L. Phillips, *Laser Beam Propagation through Random Media* (SPIE Press, Bellingham, WA, 1998).
- [5] L. C. Andrews, R. L. Phillips, and C. Y. Hopen, *Laser Beam Scintillation with Applications* (SPIE Press, Bellingham, WA, 2001).
- [6] F. R. Giorgetta, W. C. Swann, L. C. Sinclair, E. Baumann, I. Coddington, and N. R. Newbury, *Nat. Photon.* **7**, 434 (2013).
- [7] G. I. Taylor, *Proc. R. Soc., Ser. A* **164**, 476 (1938).
- [8] G. M. B. Bouricius and S. F. Clifford, *J. Opt. Soc. Am.* **60**, 1484 (1970).
- [9] S. F. Clifford, G. M. B. Bouricius, G. R. Ochs, and M. H. Ackley, *J. Opt. Soc. Am.* **61**, 1279 (1971).
- [10] J. W. Armstrong and R. A. Sramek, *Radio Sci.* **17**, 1579 (1982).
- [11] H. Matsumoto and K. Tsukahara, *Appl. Opt.* **23**, 3388 (1984).
- [12] D. F. Buscher, J. T. Armstrong, C. A. Hummel, A. Quirrenbach, D. Mozurkewich, K. J. Johnston, C. S. Denison, M. M. Colavita, and M. Shao, *Appl. Opt.* **34**, 1081 (1995).
- [13] C. Y. Young, L. C. Andrews, and A. Ishimaru, *Appl. Opt.* **37**, 7655 (1998).
- [14] K. Djerroud, O. Acef, A. Clairon, P. Lemonde, C. N. Man, E. Samain, and P. Wolf, *Opt. Lett.* **35**, 1479 (2010).
- [15] R. P. Linfield, M. M. Colavita, and B. F. Lane, *Astrophys. J.* **554**, 505 (2001).
- [16] C. S. Gardner, *Appl. Opt.* **15**, 2539 (1976).
- [17] L. Kral, I. Prochazka, and K. Hamal, *Opt. Lett.* **30**, 1767 (2005).
- [18] A. Wheelon, N. Short, and C. Townes, *Astrophys. J., Suppl. Ser.* **172**, 720 (2007).
- [19] M. M. Colavita, M. Shao, and D. H. Staelin, *Appl. Opt.* **26**, 4106 (1987).
- [20] M. Bester, W. Danchi, C. Degiacomi, L. Greenhill, and C. Townes, *Astrophys. J.* **392**, 357 (1992).
- [21] B. Sprenger, J. Zhang, Z. H. Lu, and L. J. Wang, *Opt. Lett.* **34**, 965 (2009).
- [22] S. R. Jefferts, M. A. Weiss, J. Levine, S. Dilla, E. W. Bell, and T. E. Parker, *IEEE Trans. Instrum. Meas.* **46**, 209 (1997).
- [23] M. Kihara, A. Imaoka, M. Imae, and K. Imamura, *IEEE Trans. Instrum. Meas.* **50**, 709 (2001).
- [24] J. Ye, J. Peng, R. Jones, K. Holman, J. Hall, D. Jones, S. Diddams, J. Kitching, S. Bize, J. Bergquist, L. Hollberg, L. Robertsson, and L. Ma, *J. Opt. Soc. Am. B* **20**, 1459 (2003).
- [25] I. Coddington, W. C. Swann, L. Lorini, J. C. Bergquist, Y. Le Coq, C. W. Oates, Q. Quraishi, K. S. Feder, J. W. Nicholson, P. S. Westbrook, S. A. Diddams, and N. R. Newbury, *Nat. Photon.* **1**, 283 (2007).
- [26] N. R. Newbury, P. A. Williams, and W. C. Swann, *Opt. Lett.* **32**, 3056 (2007).
- [27] P. A. Williams, W. C. Swann, and N. R. Newbury, *J. Opt. Soc. Am. B* **25**, 1284 (2008).
- [28] F. Kefelian, O. Lopez, H. F. Jiang, C. Chardonnet, A. Amy-Klein, and G. Santarelli, *Opt. Lett.* **34**, 1573 (2009).
- [29] F.-L. Hong, M. Musha, M. Takamoto, H. Inaba, S. Yanagimachi, A. Takamizawa, K. Watabe, T. Ikegami, M. Imae, Y. Fujii, M. Amemiya, K. Nakagawa, K. Ueda, and H. Katori, *Opt. Lett.* **34**, 692 (2009).
- [30] S.-C. Ebenhag, P.-O. Hedekvist, P. Jarlemark, R. Emardson, K. Jaldehag, C. Rieck, and P. Lothberg, *IEEE Trans. Instrum. Meas.* **59**, 1918 (2010).
- [31] D. Hou, P. Li, C. Liu, J. Zhao, and Z. Zhang, *Opt. Express* **19**, 506 (2011).
- [32] G. Marra, R. Slavík, H. S. Margolis, S. N. Lea, P. Petropoulos, D. J. Richardson, and P. Gill, *Opt. Lett.* **36**, 511 (2011).

- [33] K. Predehl, G. Grosche, S. M. F. Raupach, S. Droste, O. Terra, J. Alnis, T. Legero, T. W. Hänsch, T. Udem, R. Holzwarth, and H. Schnatz, *Science* **336**, 441 (2012).
- [34] S.-C. Ebenhag, P. O. Hedekvist, and K. Jaldehag, *NCSL Intl. Meas. J. Meas. Sci.* **8**, 52 (2013).
- [35] V. I. Tatarski, *Wave Propagation in a Turbulent Medium* (McGraw-Hill, New York, 1961).
- [36] R. S. Lawrence and J. W. Strohbehn, *Proc. IEEE* **58**, 1523 (1970).
- [37] S. F. Clifford, *J. Opt. Soc. Am.* **61**, 1285 (1971).
- [38] D. P. Greenwood and D. O. Tarazano, *A Proposed Form for the Atmospheric Microtemperature Spatial Spectrum in the Input Range* (Rome Air Development Center, Griffiss Air Force Base, New York, 1974).
- [39] J. M. Conan, G. Rousset, and P.-Y. Madec, *J. Opt. Soc. Am. A* **12**, 1559 (1995).
- [40] P. E. Ciddor, *Appl. Opt.* **35**, 1566 (1996).
- [41] D. L. Fried, *Proc. IEEE* **55**, 57 (1967).
- [42] C. Y. Young, A. Ishimaru, and L. C. Andrews, *Appl. Opt.* **35**, 6522 (1996).
- [43] C. H. Liu and K. C. Yeh, *Radio Sci.* **14**, 925 (1979).
- [44] K. D. Ridley, *Appl. Opt.* **50**, 5085 (2011).
- [45] I. Coddington, W. C. Swann, L. Nenadovic, and N. R. Newbury, *Nat. Photon.* **3**, 351 (2009).
- [46] J. L. Caccia, M. Azouit, and J. Vernin, *Appl. Opt.* **26**, 1288 (1987).
- [47] IEEE Std 1139-1999 1 (1999).
- [48] J. H. Shapiro, *J. Opt. Soc. Am.* **61**, 492 (1971).
- [49] J. H. Shapiro and A. L. Puryear, *J. Opt. Commun. Networking* **4**, 947 (2012).
- [50] A. L. Puryear, J. H. Shapiro, and R. R. Parenti, *Proc. SPIE 8517, Laser Commun. Propag. Atmosphere and Oceans 85170N* (2012).
- [51] J. Minet, M. A. Voronstov, E. Polnau, and D. Dolfi, *J. Opt.* **15**, 022401 (2013).
- [52] R. R. Parenti, J. M. Roth, J. H. Shapiro, F. G. Walther, and J. A. Greco, *Opt. Express* **20**, 21635 (2012).
- [53] C. W. Chou, D. B. Hume, J. C. J. Koelemeij, D. J. Wineland, and T. Rosenband, *Phys. Rev. Lett.* **104**, 070802 (2010).
- [54] M. Takamoto, T. Takano, and H. Katori, *Nat. Photon.* **5**, 288 (2011).
- [55] T. L. Nicholson, M. J. Martin, J. R. Williams, B. J. Bloom, M. Bishof, M. D. Swallows, S. L. Campbell, and J. Ye, *Phys. Rev. Lett.* **109**, 230801 (2012).
- [56] N. Hinkley, J. A. Sherman, N. B. Phillips, M. Schioppo, N. D. Lemke, K. Beloy, M. Pizzocaro, C. W. Oates, and A. D. Ludlow, *Science* **341**, 1215 (2013).
- [57] U. Frisch, P.-L. Sulem, and M. Nelkin, *J. Fluid Mech.* **87**, 719 (1978).